Acta Mech 228:2377–2390 (2017)
DOI 10.1007/s00707-017-1812-9

REVIEW ARTICLE

Georgios I. Giannopoulos · Stylianos K. Georgantzinos

Establishing detection maps for carbon nanotube mass sensors: molecular versus continuum mechanics

Received: 31 August 2016 / Revised: 28 December 2016 / Published online: 11 February 2017

Abstract In this work, the mass-sensing ability and the corresponding detection efficiency of a fully clamped single-walled carbon nanotube (SWCNT) are investigated through a free vibration analysis, by utilizing mainly a molecular mechanics (MM) formulation and secondarily a continuum mechanics (CM) analytical approximation. The MM method is based on representing the SWCNT as a three-dimensional (3D) finite element frame of point masses and linear springs, while the CM one is grounded on the Euler–Bernoulli beam theory. The overall effort is focused on obtaining detection maps, based on natural frequency data which are capable of leading to the straightforward identification of an unknown mass attached to the external surface of the candidate SWCNT sensor. For this reason, the SWCNT relative natural frequency shifts due to the mass addition, regarding specific modes of vibration and for a variety of mass magnitude and position combinations, are calculated beforehand. Then, the magnitude as well as the position of the added mass may be graphically found by superposing the arisen relative natural frequency shift variations in common contour diagrams. Some results from the open literature are utilized to confirm the predictive performance of the proposed MM method concerning the free vibration of pure SWCNTs, while the MM and CM established detection maps are set in contrast to examine whether a mass nanosensor may be satisfactorily treated in a continuum manner.

1 Introduction

A wide interest has been recently devoted to the study of sensors which are capable of detection in nanoscale, commonly known as nanosensors. Nanosensors are usually nanosystems, the major components of which are usually typical nanomaterials such as nanotubes or other graphene-like materials. Such nanodevices are used to monitor and detect any physical, chemical and biological signals and then to convey the sensory information from the nanoscopic to the macroscopic world. Their use principally includes various medicinal purposes involving the potential of accurate identification of specific cells, particles or regions within the body by measuring changes in mass [1], concentration [2], displacement [3], velocity [4], pressure [5], electrical forces

G. I. Giannopoulos (✉)
Materials Science Laboratory, Department of Mechanical Engineering,
Technological Educational Institute of Western Greece, 1 Megalou Alexandrou Street, 26334 Patras, Greece
E-mail: ggiannopoulos@teiwest.gr
Tel.: +302610369273

G. I. Giannopoulos
Department of Materials Science, University of Patras, 26504 Patras, Greece

S. K. Georgantzinos
Machine Design Laboratory, Department of Mechanical Engineering and Aeronautics,
University of Patras, Rio, 26500 Patras, Greece
E-mail: sgeor@mech.upatras.gr

[6], magnetic forces [6] and temperature [3]. In particular, the use of carbon allotropes such as carbon nanotubes, graphene nanoribbons, fullerenes and carbon nanofibers has attracted a lot of attention in the field of sensor nanotechnology [7,8], due to their exceptional mechanical, thermal, electrical, optical and electrochemical properties. Among all nanomaterials, the carbon nanotubes seem to play a key role on the development of the modern generation of sensors [9]. In this context, the special SWCNT vibrational characteristics should be taken into advantage. Experimental verification of carbon nanotube-based mass sensors has already been demonstrated [10–12].

The vibration behavior of carbon nanotubes has been investigated by using a variety of theoretical approaches which are based on atomistic modeling via molecular dynamics (MD) or MM, CM and nanoscale CM-based modeling [13]. Li and Chou [14] have employed an atomistic structural mechanics modeling to predict the fundamental frequencies of cantilevered and SWCNTs. Fakhrabadi et al. have studied the vibrational properties of junctioned [15] and coiled carbon nanotubes [16] as well as carbon nanocones [17] by using an MM finite element method. Chowdhury et al. [18] have investigated the vibrational properties of zigzag and armchair SWCNTs using an MM approach. Ansari et al. [19] have adopted a nonlocal shell model as well as MD simulations to study the free vibrations of SWCNTs. Kim et al. [20] have analyzed the chirality and length dependence of the vibrational behavior of SWCNTs using an atomistic elastic network model. Annin et al. [21] have utilized a beam-based MM method to determine the natural frequencies of SWCNTs with twisted ends. Lee and Lee [22] have performed a modal analysis of SWCNTs and single- walled carbon nanocones using beam-like finite elements to simulate interatomic interactions. Kiani [23] has used a nonlocal Rayleigh beam model to develop discrete and continuous models for analyzing vibrational behavior of ensembles of SWCNTs under dynamic loads. Imani Yengejeh et al. [24] have developed several MM-based finite element models of homogenous straight and curved SWCNTs. Imani Yengejeh et al. [25] as well as Motamedi et al. [26] have studied the vibrational behavior of SWCNT junctions using MM-based approaches. Gajbhiye and Singh [27] have addressed questions on the vibration characteristics of open- and capped-end SWCNTs using a multi-scale analysis based on an atomistic finite element method. Askari et al. [28] have combined the nonuniform rational B-spline with the Euler–Bernoulli beam theory to study the nonlinear vibration of carbon nanotubes with different shapes of curvature. Patel and Joshi [29] have studied the effect of defects on the vibration characteristics of double-walled carbon nanotubes (DWCNTs) using a beam-based MM approach. Lastly, Amjadipour et al. [30] have examined the combination effects of both initial curvature and vacancy defects on vibrational behavior of SWCNTs, utilizing the MD and the finite element method.

Despite the fact that there are numerous studies associated with the vibration behavior of pure carbon nanotubes, the contribution of their vibration signatures on mass sensing and detection has not been exploited to the same extent. Li et al. [1] have studied the free vibration and mass detection of carbon nanotube-based sensors via nonlocal beam theory. Fakhrabadi et al. [31] have examined the application of carbon nanotubes as mass sensors using a MM-based finite element modeling. Ouaked and Younis [32,33] have examined the dynamics of electrically actuated slacked and initially curved SWCNTs. Joshi et al. [34] have explored the use of chiral SWCNTs as mass sensors using an atomistic finite element model based on an MM approach. Finally, following a similar approach, Patel and Joshi [35] have explored DWCNTs with mono-atomic vacancies as mass-sensing devices.

To expand the relevant research, the present work aims to provide a complete process of establishing novel mass detection maps for SWCNT sensors. An atomistic MM method is utilized for this purpose, which utilizes 3D point mass- and linear spring-like finite elements to describe the potential field within a SWCNT-added mass system. To the authors' best knowledge, it is the first time that vibrational behavior of carbon nanotubes is tested via the specific MM formulation. Thus, some indicative comparisons concerning the performance of the proposed numerical scheme are presented. Contour maps of SWCNT relative frequency shifts regarding different modes of vibration due to the particle attachment are combined in common diagrams to enable simple identification of the magnitude and the position of the added mass. Finally, an Euler–Bernoulli-based CM formulation is being carried out to establish the detection maps of the same SWCNT mass sensor problem. The effectiveness of CM in representing the vibration behavior of nanostructured sensors is discussed.

2 Molecular mechanics

The free vibration behavior of the SWCNT-added mass system is approached by the implementation of an atomistic, structural mechanics formulation which is based on the use of spring- and mass-like 3D finite elements.

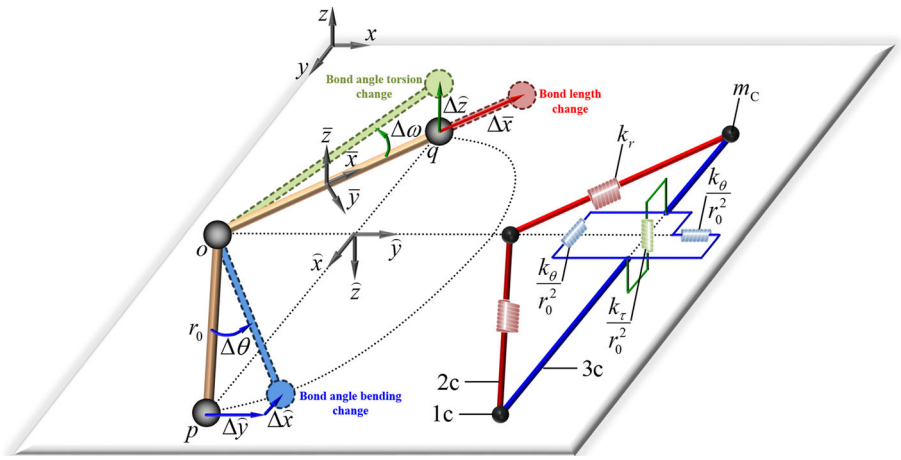

Fig. 1 Molecular mechanics analysis by using point mass- and linear spring-like finite elements

2.1 Molecular theory

Since van der Waals forces in an SWCNT are negligible, its total potential energy U_{tot} may be expressed as [36]:

$$U_{\text{tot}} = \sum U_r + \sum U_\theta + \sum U_\varphi + \sum U_\omega, \tag{1}$$

where U_r, U_θ, U_φ and U_ω are the interatomic interaction potential energies due to the bond length change, angle bending change, dihedral angle torsion change and out-of-plane torsion change, respectively.

It is computationally convenient to combine potential terms U_ϕ and U_ω in the single term $U_\tau = U_\varphi + U_\omega$ which describes the energy due to the total bond angle torsion change. Then, according to the universal force field (UFF) [36], the following harmonic forms of the potential energies may be adopted for small strains:

$$U_r = \frac{1}{2}k_r(\Delta r)^2, \quad U_\theta = \frac{1}{2}k_\theta(\Delta\theta)^2, \quad U_\tau = \frac{1}{2}k_\tau(\Delta\varphi)^2, \tag{2}$$

where Δr, $\Delta\theta$ and $\Delta\varphi$ are the bond length, angle bending and angle torsion changes shown in Fig. 1, while the stiffness terms k_r, k_θ and k_τ are the bond length, angle bending and angle torsion resistance force constants taken equal to 652 nNnm^{-1}, 0.876 nN nm rad^{-2}, and 0.272 nN nm rad^{-2} [37], respectively.

It should be mentioned that the UFF has previously been proven to provide accurate predictions regarding carbon nanotubes [13,14,18,34], and thus, it is preferred in the present analysis.

2.2 Development of molecular mechanics equations

Assume that the equilibrium state of the C–C–C bonds in an SWCNT is described in (x, y, z) space by the atomic position points p, o and q as Fig. 1 illustrates. The bond length change and both the bond angle interactions are analyzed in the $(\bar{x}, \bar{y}, \bar{z})$ and $(\widehat{x}, \widehat{y}, \widehat{z})$ local coordinate systems, respectively, placed as Fig. 1 illustrates. For small strains and by assuming that the equilibrium bond length is $|op| = |oq| = r_0 = 0.1421$ nm, there is:

$$\Delta r = \Delta\bar{x}, \quad \Delta\theta = \frac{\sqrt{(\Delta\widehat{x})^2 + (\Delta\widehat{y})^2}}{r_0}, \quad \Delta\varphi = \frac{\Delta\widehat{z}}{r_0}, \tag{3}$$

where $\Delta\bar{x}$, both $\Delta\widehat{x}$ and $\Delta\widehat{y}$, and $\Delta\widehat{z}$ are the resultant displacement changes due to the bond length, angle bending and angle torsion changes, respectively.

An efficient, in terms of computer implementation, total potential energy expression is found by substituting Eqs. (2) and (3) in Eq. (1):

$$U_{\text{tot}} = \overbrace{\sum \frac{1}{2}k_r(\Delta\bar{x})^2}^{\text{Bond length change}} + \overbrace{\sum \frac{1}{2}\frac{k_\theta}{r_0^2}(\Delta\widehat{x})^2 + \sum \frac{1}{2}\frac{k_\theta}{r_0^2}(\Delta\widehat{y})^2}^{\text{Bond angle bending change}} + \overbrace{\sum \frac{1}{2}\frac{k_\tau}{r_0^2}(\Delta\widehat{z})^2}^{\text{Bond angle torsion change}}. \tag{4}$$

In the above equation, the second derivatives of the first, both second and third, and fourth potential energy terms with respect to the corresponding displacement changes yield the stiffness coefficients k_r, k_θ/r_0^2 and k_τ/r_0^2, respectively.

2.3 Finite element implementation

Mass- and spring-like elements with three degrees of freedom per node, i.e., three translations, are utilized for the representation of the SWCNT-added mass system.

Any mass contribution in the SWCNT-added mass system is modeled by the point mass element indicated by 1c in Fig. 1, with the following stiffness matrix with respect to (x, y, z):

$$\mathbf{M}_{1c} = \begin{bmatrix} m & 0 & 0 & 0 & 0 & 0 \\ 0 & m & 0 & 0 & 0 & 0 \\ 0 & 0 & m & 0 & 0 & 0 \\ 0 & 0 & 0 & 0 & 0 & 0 \\ 0 & 0 & 0 & 0 & 0 & 0 \\ 0 & 0 & 0 & 0 & 0 & 0 \end{bmatrix}, \tag{5}$$

where, given that the atomic mass of carbon is $m_c = 1.9943 \times 10^{-26}$ kg and by suggesting that the added mass is m_a, the mass coefficient m is:

$$m = \begin{cases} m_c & \text{at the single carbon atoms,} \\ m_c + m_a & \text{at the added mass position.} \end{cases} \tag{6}$$

Furthermore, the bond length change is modeled by the linear spring element indicated by 2c in Fig. 1, with the following stiffness matrix with respect to $(\bar{x}, \bar{y}, \bar{z})$:

$$\bar{\mathbf{K}}_{2c} = \begin{bmatrix} k_r & 0 & 0 & -k_r & 0 & 0 \\ 0 & 0 & 0 & 0 & 0 & 0 \\ 0 & 0 & 0 & 0 & 0 & 0 \\ -k_r & 0 & 0 & k_r & 0 & 0 \\ 0 & 0 & 0 & 0 & 0 & 0 \\ 0 & 0 & 0 & 0 & 0 & 0 \end{bmatrix}. \tag{7}$$

Finally, both the bond bending angle and torsion angle change are modeled by the linear spring element indicated by 3c in Fig. 1, with the following three-parameter dependent stiffness matrix with respect to $(\widehat{x}, \widehat{y}, \widehat{z})$:

$$\widehat{\mathbf{K}}_{3c} = \begin{bmatrix} \frac{k_\theta}{r_0^2} & 0 & 0 & -\frac{k_\theta}{r_0^2} & 0 & 0 \\ 0 & \frac{k_\theta}{r_0^2} & 0 & 0 & -\frac{k_\theta}{r_0^2} & 0 \\ 0 & 0 & \frac{k_\tau}{r_0^2} & 0 & 0 & -\frac{k_\tau}{r_0^2} \\ -\frac{k_\theta}{r_0^2} & 0 & 0 & \frac{k_\theta}{r_0^2} & 0 & 0 \\ 0 & -\frac{k_\theta}{r_0^2} & 0 & 0 & \frac{k_\theta}{r_0^2} & 0 \\ 0 & 0 & -\frac{k_\tau}{r_0^2} & 0 & 0 & \frac{k_\tau}{r_0^2} \end{bmatrix}. \tag{8}$$

Figure 2 illustrates the finite element model and the arrangement of the 1b, 2b and 3b elements of the fully clamped SWCNT-added mass system which is studied in the present work. The diameter and the length of the SWCNT are denoted as D and L, respectively, while the position of the added mass m_a is defined via the minimum axial distance from the supports which is denoted as l_a.

Utilizing the well-known atomistic geometry of the SWCNT as well as its edge support conditions and assembling all the elemental stiffness and mass matrix equations, the following system of algebraic equations with respect to the global coordinate system (x, y, z) arises:

$$\mathbf{M}\ddot{\mathbf{U}} + \mathbf{K}\mathbf{U} = \mathbf{0}, \tag{9}$$

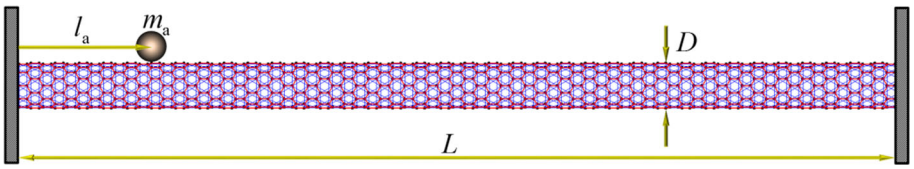

Fig. 2 Molecular mechanics treatment of the SWCNT-added mass system

where **M**, **K** and **U** are the assembled mass matrix, stiffness matrix and displacement vector, respectively. The dot denotes the derivative with respect to the time.

Evidently, the **U** vector is constructed by assembling all the elemental displacement vectors **u**. The displacement vector for an adopted finite element with nodes denoted as 1 and 2 may be written as:

$$\mathbf{u} = \left[u_x^{(1)} \quad u_y^{(1)} \quad u_z^{(1)} \quad u_x^{(2)} \quad u_y^{(2)} \quad u_z^{(2)}\right]^{\mathrm{T}}, \tag{10}$$

where u_x, u_y and u_y represent the three translational degrees of freedom at each node in the global coordinate system.

By assuming a harmonic motion of angular frequency ω_m of a SWCNT with an added mass m_{a} at l_{a}, Eq. (9) may be rewritten as:

$$[\mathbf{K} - \omega_m^2 \mathbf{M}]\mathbf{U} = \mathbf{0}. \tag{11}$$

Last equation may lead to the estimation of the eigenvalue, i.e., the natural angular frequency ω_m, and the corresponding eigenvector, i.e., mode shape, for the mth mode of vibration. The natural frequency f_m may be calculated by the angular one via the relationship:

$$f_m = \frac{\omega_m}{2\pi}. \tag{12}$$

Finally, the relative frequency shift f_m^*, which is observed due to the added mass m_{a} at l_{a}, is defined as:

$$f_m^* = \frac{{}^{\mathrm{p}}f_m - f_m}{{}^{\mathrm{p}}f_m}, \tag{13}$$

where ${}^{\mathrm{p}}f_m$ is the natural frequency of the mth mode of vibration of the pure SWCNT.

3 Continuum mechanics

Additionally, in order to conduct some qualitative comparisons, the SWCNT is considered to behave as a clamped–clamped beam with a lumped mass along its length as Fig. 3 illustrates.

To enable the application of the Euler–Bernoulli beam theory, the SWCNT is considered as a hollow beam-like cylinder of cross-sectional area A, second moment of area I, elastic modulus E and linear density μ. Under these assumptions, the transverse free vibration of the beam may be described by the partial differential equation:

$$EI\frac{\partial^4 y}{\partial x^4} + \mu\frac{\partial^2 y}{\partial t^2} = 0, \tag{14}$$

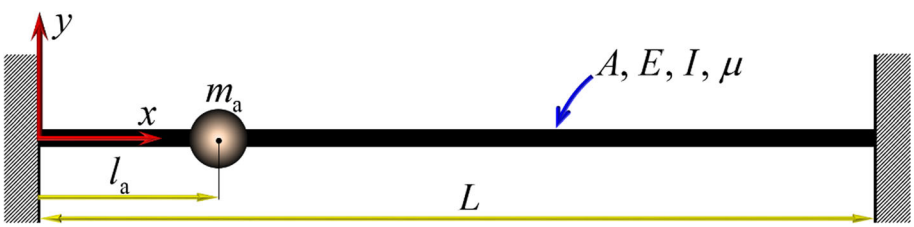

Fig. 3 Continuum mechanics treatment of the SWCNT-added mass system

where $y = (x, t)$ is the transverse displacement of the beam, x is the longitudinal coordinate of the beam, and t is the time.

By assuming that initial transverse displacement, bending angle, bending moment and shear force at $x = 0$ are y_0, ϕ_0, M_0 and Q_0, respectively, then the state parameter $y(x)$ and $\phi(x)$ may be expressed, respectively, as [38]:

$$y(x) = y_0 S(\kappa_m x) + \phi_0 \kappa_m^{-1} T(\kappa_m x) + \frac{M_0}{EI}\kappa_m^{-2} U(\kappa_m x) + \frac{Q_0}{EI}\kappa_m^{-3} V(\kappa_m x) + \frac{m_a}{\mu}\kappa_m y(l_a) V(\kappa_m (x - l_a)), \tag{15}$$

$$\phi(x) = y_0 \kappa_m V(\kappa_m x) + \phi_0 S(\kappa_m x) + \frac{M_0}{EI}\kappa_m^{-1} T(\kappa_m x) + \frac{Q_0}{EI}\kappa_m^{-2} U(\kappa_m x) + \frac{m_a}{\mu}\kappa_m^2 y(l_a) U(\kappa_m (x - l_a)), \tag{16}$$

where the functions S, T, U and V are given by:

$$\begin{Bmatrix} S(\chi) \\ T(\chi) \\ U(\chi) \\ V(\chi) \end{Bmatrix} = \frac{1}{2}\begin{Bmatrix} \cosh\chi + \cos\chi \\ \sinh\chi + \sin\chi \\ \cosh\chi - \cos\chi \\ \sinh\chi - \sin\chi \end{Bmatrix}, \tag{17}$$

while κ_m is a frequency parameter which is associated with the natural angular frequency according to:

$$\omega_m = \kappa_m^2 \sqrt{\frac{EI}{\mu}}. \tag{18}$$

Since the beam-like SWCNT is clamped at $x = 0$, there is $y_0 = \phi_0 = 0$, and therefore, $y(x)$ and $\phi(x)$ are reduced, respectively, to:

$$y(x) = \frac{M_0}{EI}\kappa_m^{-2} U(\kappa_m x) + \frac{Q_0}{EI}\kappa_m^{-3} V(\kappa_m x) + \frac{m_a}{\mu}\kappa_m y(l_a) V(\kappa_m (x - l_a)), \tag{19}$$

$$\phi(x) = \frac{M_0}{EI}\kappa_m^{-1} T(\kappa_m x) + \frac{Q_0}{EI}\kappa_m^{-2} U(\kappa_m x) + \frac{m_a}{\mu}\kappa_m^2 y(l_a) U(\kappa_m (x - l_a)). \tag{20}$$

Since the deflection and slope are zero at the right clamped end of the beam-like SWCNT as well, i.e., $y(L) = \phi(L) = 0$, Eqs. (19) and (20) lead, respectively, to:

$$\frac{M_0}{EI} U(\kappa_m L) + \frac{Q_0}{EI}\kappa_m^{-1} V(\kappa_m L) + \frac{m_a}{\mu}\kappa_m^3 y(l_a) V(\kappa_m (L - l_a)) = 0, \tag{21}$$

$$\frac{M_0}{EI} T(\kappa_m L) + \frac{Q_0}{EI}\kappa_m^{-1} U(\kappa_m L) + \frac{m_a}{\mu}\kappa_m^3 y(l_a) U(\kappa_m (L - l_a)) = 0. \tag{22}$$

To define $y(l_a)$, Eq. (19) is applied for $x = l_a$, giving:

$$y(l_a) = \frac{M_0}{EI}\kappa_m^{-2} U(\kappa_m l_a) + \frac{Q_0}{EI}\kappa_m^{-3} V(\kappa_m l_a). \tag{23}$$

By substituting Eq. (23) into Eqs. (21) and (22), the following homogenous system arises:

$$M_0\left[U(\kappa_m L) + \frac{m_a}{\mu}\kappa_m V(\kappa_m (L - l_a)) U(\kappa_m l_a)\right] + Q_0\left[\kappa_m^{-1} V(\kappa_m L) + \frac{m_a}{\mu} V(\kappa_m (L - l_a)) V(\kappa_m l_a)\right] = 0, \tag{24}$$

$$M_0\left[T(\kappa_m L) + \frac{m_a}{\mu}\kappa_m U(\kappa_m (L - l_a)) U(\kappa_m l_a)\right] + Q_0\left[\kappa_m^{-1} U(\kappa_m L) + \frac{m_a}{\mu} U(\kappa_m (L - l_a)) V(\kappa_m l_a)\right] = 0. \tag{25}$$

The last system of equations has a nontrivial solution if and only if its determinant is zero, i.e.,

$$\begin{vmatrix} U(\kappa_m L) + \frac{m_a}{\mu}\kappa_m V(\kappa_m(L-l_a))\, U(\kappa_m l_a)\, \kappa_m^{-1} V(\kappa_m L) + \frac{m_a}{\mu} V(\kappa_m(L-l_a))\, V(\kappa_m l_a) \\ T(\kappa_m L) + \frac{m_a}{\mu}\kappa_m U(\kappa_m(L-l_a))\, U(\kappa_m l_a)\, \kappa_m^{-1} U(\kappa_m L) + \frac{m_a}{\mu} U(\kappa_m(L-l_a))\, V(\kappa_m l_a) \end{vmatrix} = 0. \tag{26}$$

The frequency parameter κ_m with $m = 1, 2, 3, \ldots$ is the root of the last equation. By substituting the generalized Eq. (12) and the analytical Eq. (18) into the generalized Eq. (13), the following expression regarding the analytical estimation of the natural frequency shift of the beam-like SWCNT due to the mass attachment is obtained:

$$f_m^* = 1 - \left(\frac{\kappa_m}{{}^{\mathrm{p}}\kappa_m}\right)^2, \tag{27}$$

where ${}^{\mathrm{p}}\kappa_m$ is the frequency parameter for the mth mode of vibration of the pure SWCNT and may be calculated by setting m_a to zero in Eq. (26).

Note that the first term of Eq. (27), which has to be calculated, is a relative natural frequency parameter, and thus, it may be reduced to an expression which does not contain the flexural rigidity EI and the linear density μ included in Eq. (18). As a result, its calculation does not require the input of the section and material properties of the beam-like SWCNT.

4 Results and discussion

The sensing ability of the, fully clamped, zigzag (10,0) SWCNT is under investigation. The mean diameter of the nanotube is $D = 0.7834$ nm. In order to achieve an aspect ratio L/D around 20, which provides enough room for possible external particle attachments, its free length is taken equal to $L = 15.49$ nm. For such a length, the specific nanotube consisted of $N = 1480$ carbon atoms. The SWCNT is chosen to be clamped in both sides, since such a support provides better control and protection for the candidate sensor while leads to higher natural frequency changes in comparison with other less stiff supports.

During the presentation of the results, it is found convenient to describe the magnitude and the position of the added mass via the following dimensionless parameters, respectively:

$$m^* = m_a/m_c, \quad l^* = l_a/L. \tag{28}$$

For comparison reasons, the output illustrations, presented in the following, regarding both MM and CM methods are extracted by utilizing the same input data points, i.e., combinations of magnitude and position of the added mass. Specifically, the dimensionless input data points (m^*, l^*) which are described by the following equations are adopted:

$$m^* = 5(1+i), \quad l^* = (1+3j)r_0/L, \tag{29}$$

where $i, j = 0, 1, 2, \ldots, 19$.

The attachment of an external mass m_a to the (10,0) SWCNT which is higher than $100m_c$ is considered rather unrealistic and out of practical interest, given the relevant geometric, stability and strength restrictions, and thus, the investigation of the cases with $m^* > 100$ is avoided. In addition, due to the symmetry of the problem, the maximum tested dimensionless value regarding the position of the mass is selected to be $l^* = 0.5$.

4.1 Molecular mechanics predictions

To evaluate the performance of the proposed finite element MM method before starting investigating the core problem of the SWCNT mass sensor, Fig. 4 is presented. The specific figure illustrates the variation of the fundamental natural frequency with respect to the aspect ratio of two different in terms of chirality and diameter SWCNTs, i.e., the zigzag (10,0) and the armchair (8,8). Moreover, two boundary condition cases are tested, i.e., the clamped–clamped and the free–free edge supports. Despite the overall similarity between the differently predicted variations, notable differences may be observed between their absolute values for a given aspect ratio due to the dissimilar theoretical background followed by each method [39]. However, it may be hypothesized that, regarding the results of the SWCNT-added mass system, such inherent differences could be minimized by utilizing the nondimensionalization described by Eq. (13).

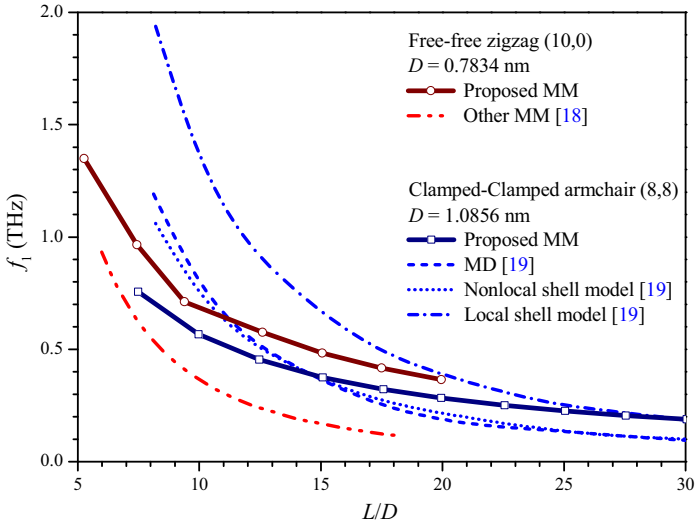

Fig. 4 Fundamental natural frequency versus aspect ratio of pure SWCNTs calculated by the proposed MM method in contrast to other corresponding numerical predictions

Next, the fully clamped (10,0) SWCNT-added mass system of $L/D \approx 20$ is considered. Given the well-known atomistic geometry of the (10,0) zigzag SWCNT, to perform the free vibration finite element analysis of the system, the use of 1480 1c, 2210 2c and 4760 3c elements is required (Fig. 2). A time of 12 s is enough to extract the first ten natural frequencies and corresponding mode shapes, using an eight-core processor at 4GHz CPU speed and a 16GB RAM, a fact that proves the computational efficiency of the proposed MM method in comparison with the MD one. Figure 5 presents the first six natural frequencies ${}^{\mathrm{p}}f_m$ and the corresponding modes shapes of the pure SWCNT. The first, third, fourth and sixth mode shapes are of the bending type, while the second and fifth are of the breathing one. It has to be noted that according to the finite element simulations, similar mode shapes appear in different directions. However, their illustration is omitted since they lead to identical natural frequencies.

Figure 6a–f illustrates the variations of the relative frequency shifts regarding the first, second, third, fourth, fifth and sixth modes of vibration, i.e., f_1^*, f_2^*, f_3^*, f_4^*, f_5^* and f_6^*, correspondingly, with respect to the dimensionless magnitude m^* and position l^* of the attached SWCNT mass. Note the schematic similarity of theses curves from $l^* = 0$ to $l^* = 0.5$ with the transverse deformations along the nanotube axial direction of the corresponding mode shapes (Fig. 5). The maximum relative frequency shifts are observed when the added mass is located at the middle of the SWCNT length L, regarding the first, second and fourth modes of vibration. In contrast the highest natural frequency changes concerning the third as well as fifth mode of vibration occurs when $l^* = 1/4,\ 3/4$. Finally, when the mass is positioned at $l^* = 3/8,\ 5/8$, the sixth natural frequency undergoes the most significant change. Evidently, the higher the magnitude of the added mass, the higher the frequency shifts regardless of the mode of vibration. Finally, the sixth and fourth bending natural frequencies exhibit the maximum change due to mass addition, while the rest four relative natural frequency shifts present maximum values of the same level.

Then, simplified contour maps for the detection of the added mass in the SWCNT may be obtained by superposing the 3d relative natural frequency shift variations of Fig. 6 in common 2d diagrams. Figure 7a–c depicts contour maps arisen by the superposition of the relative natural frequency shift colormap surfaces of the first as well as second, first as well third, and first as well as fourth modes of vibration. For convenience, all relative natural frequency shifts in Fig. 7 are expressed in percent (%).

Now, the identification of the magnitude and position of the mass may be easily realized by the obtained contours of Fig. 7 in the following manner:

(i) Suppose that the monitored natural frequencies of the SWCNT sensor are $f_1 = 0.3634$ THz, $f_2 = 0.57197$ THz, $f_3 = 0.7102$ THz, and $f_4 = 1.0838$ THz.
(ii) The corresponding natural frequencies of the pure SWCNT are ${}^{\mathrm{p}}f_1 = 0.3706$ THz, ${}^{\mathrm{p}}f_2 = 0.5825$ THz, ${}^{\mathrm{p}}f_3 = 0.7408$ THz, and ${}^{\mathrm{p}}f_4 = 1.1102$ THz (Fig. 5).
(iii) Equation (13) yields $f_1^* = 1.95\%$, $f_2^* = 1.81\%$, $f_3^* = 4.13\%$, and $f_4^* = 2.38\%$.

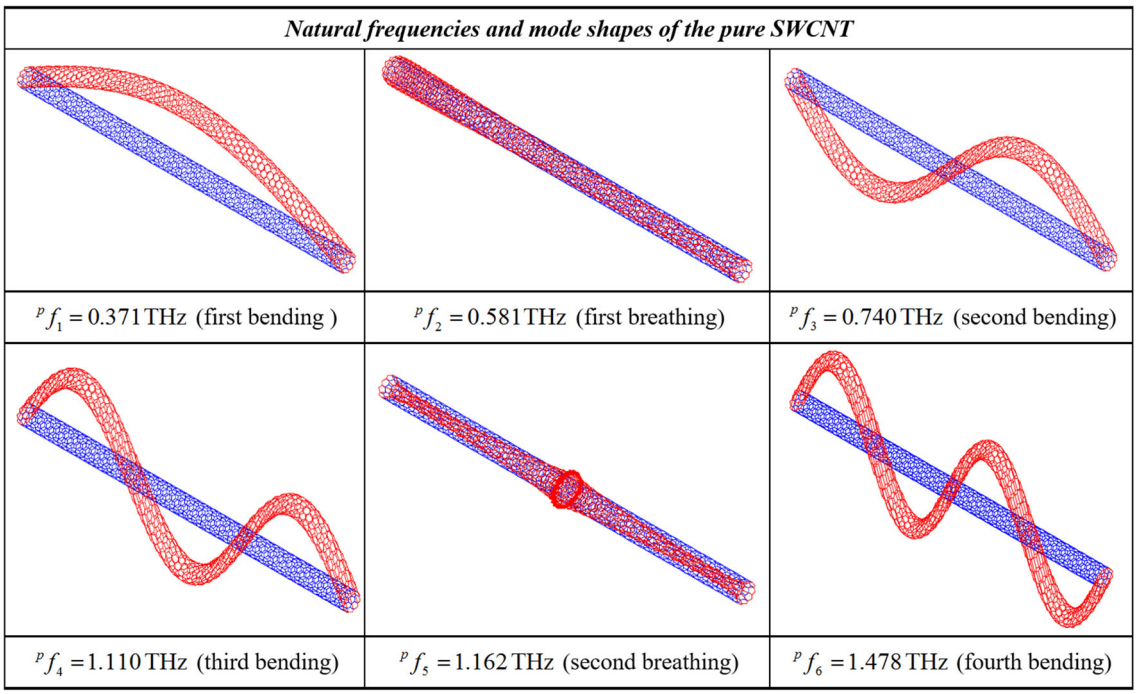

Fig. 5 First six natural frequencies and mode shapes of the pure (10,0) SWCNT according to the proposed MM method

(iv) Between the contours $f_1^* = 1.95\%$ and $f_2^* = 1.81\%$, no intersection point may be found in Fig. 7a. Between the contours $f_1^* = 1.95\%$ and $f_3 = 4.13\%$, the intersection point P_1 is found in Fig. 7b. Between the contours $f_1^* = 1.95\%$ and $f_4^* = 2.38\%$, the intersection points P_1 and P_2 are found in Fig. 7c.

(v) Therefore, the projections of intersection point P_1 on horizontal and vertical axis indicate the dimensionless magnitude and location of the attached mass, respectively, i.e., $(m^*,\ l^*) \equiv (50,\ 0.2569)$.

Note that the contours f_1^* and f_2^* in Fig. 7a, regarding the first bending and first breathing mode of vibration, respectively, are asymptotic, and therefore, the specific contour map does not permit detection of the added mass. Moreover, specific combinations of f_1^* and f_4^* contours in Fig. 7c, concerning the first and third bending modes of vibration, respectively, may lead to two different intersection points, and thus, under some circumstances, this map does not allow straightforward detection of the added mass characteristics. In contrast, Fig. 7b, which includes data of the first and second bending modes of vibration, always leads to a single intersection point independently of the combination of f_1^* and f_3^* contours and therefore seems to be the ideal detection map for the added mass.

4.2 Continuum mechanics predictions

In a second theoretical attempt, the CM-based approach is followed via Eqs. (26) and (27). In order to achieve a solution, the linear density of the SWCNT under consideration is required which may be easily estimated by $\mu = Nm_c/L$. The basic limitation of the present analytical approach is the fact that predicts only bending modes of vibration. However, the atomistic analysis shows that the two first bending modes of vibration are adequate for detecting the added mass.

Figure 8a, b depicts the analytically predicted behavior of the relative natural frequency shifts regarding the first and second bending modes of vibration, i.e., f_1^* and f_3^*, correspondingly, with respect to the dimensionless magnitude m^* and position l^* of the attached SWCNT mass. The similarity between relative natural frequency change behaviors in Figs. 6a and 8a as well as Figs. 6c and 8b becomes obvious. However, despite that the peak values obtained via MM and CM for f_1^* are almost the same, a distinct difference around 3% between maximum values in Figs. 6c and 8b may be seen. It is evident that such a difference regarding the second mode of vibration may become misleading in the detection of the added mass.

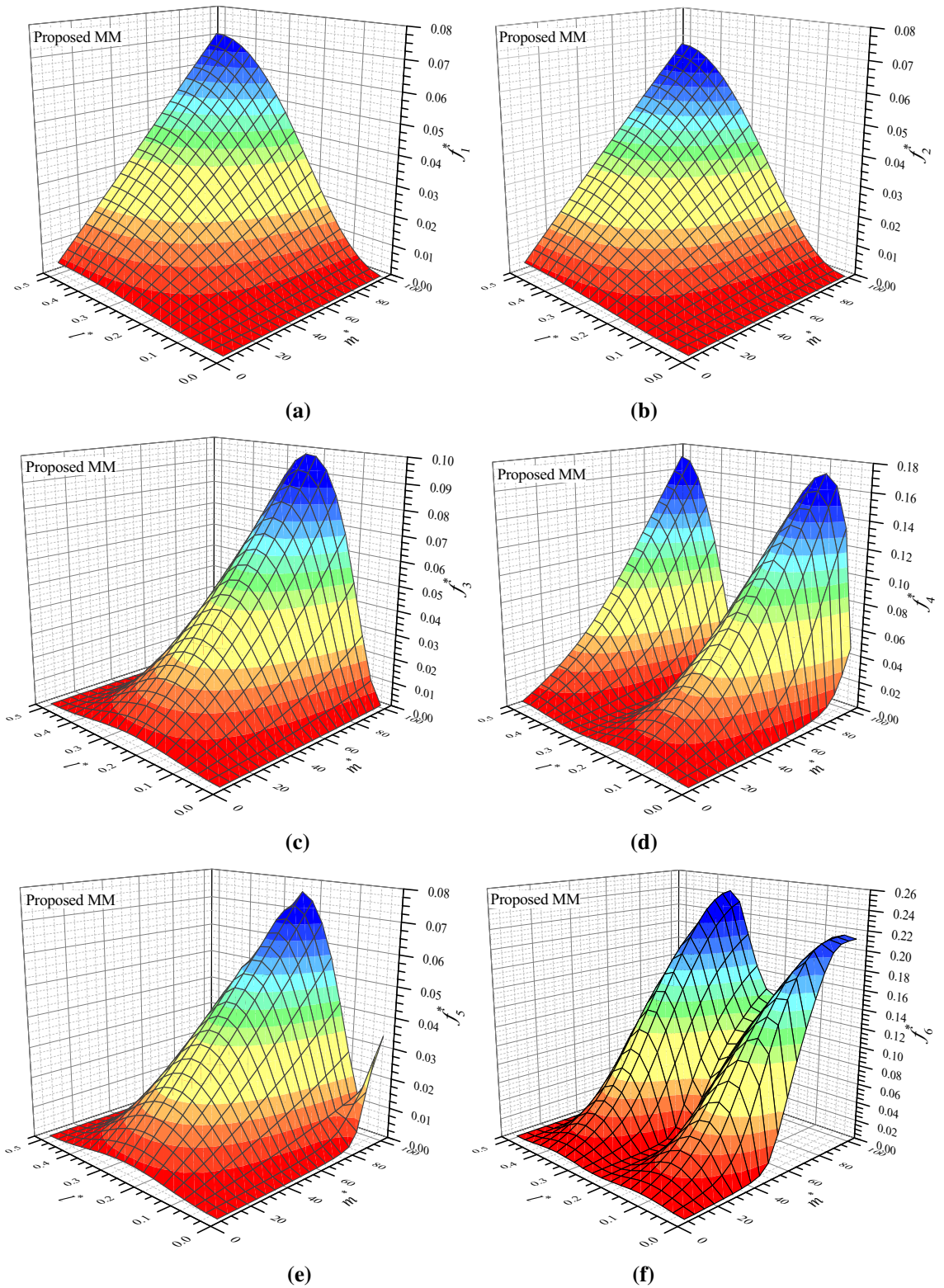

Fig. 6 Relative natural frequency shifts versus the dimensionless magnitude and position of the added mass for the **a** first, **b** second, **c** third, **d** fourth, **e** fifth and **f** sixth mode of the SWCNT-added mass vibration according to proposed MM method

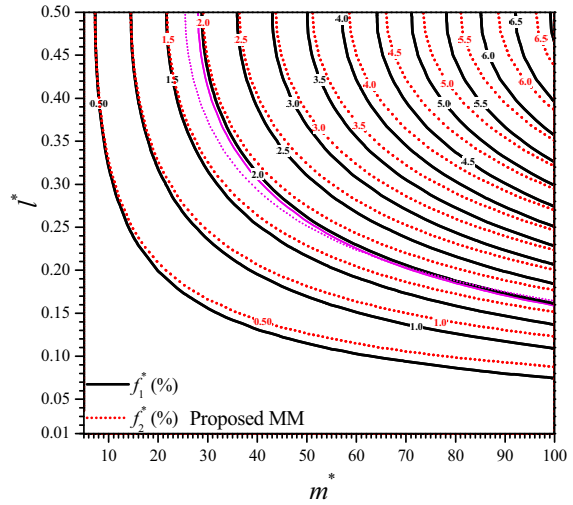

(a)

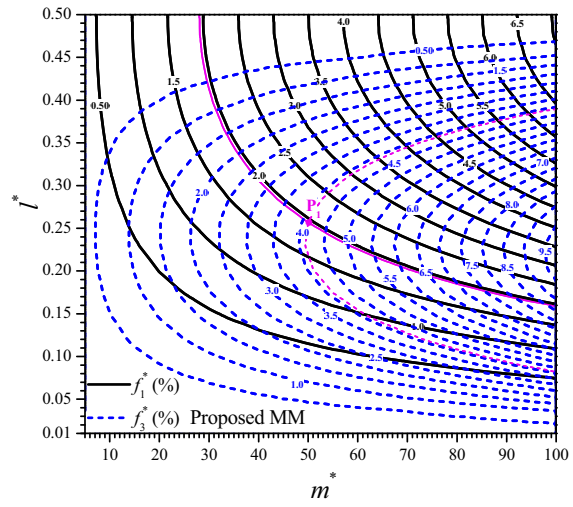

(b)

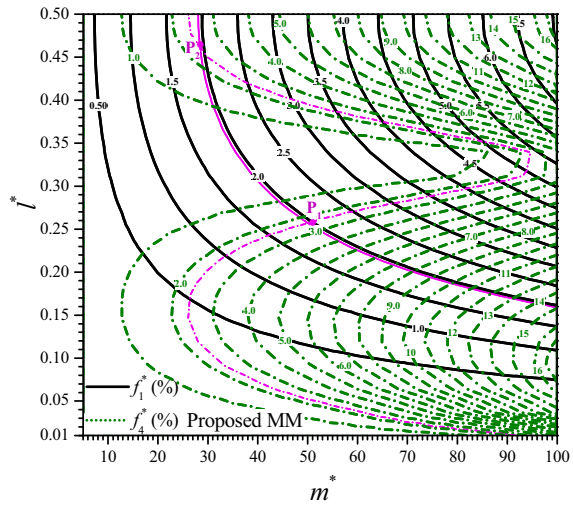

(c)

Fig. 7 Superposed contours of the relative natural frequency shifts regarding the **a** first as well as second, **b** first as well as third and **c** first as well as fourth mode of the SWCNT-added mass vibration according to the proposed MM method

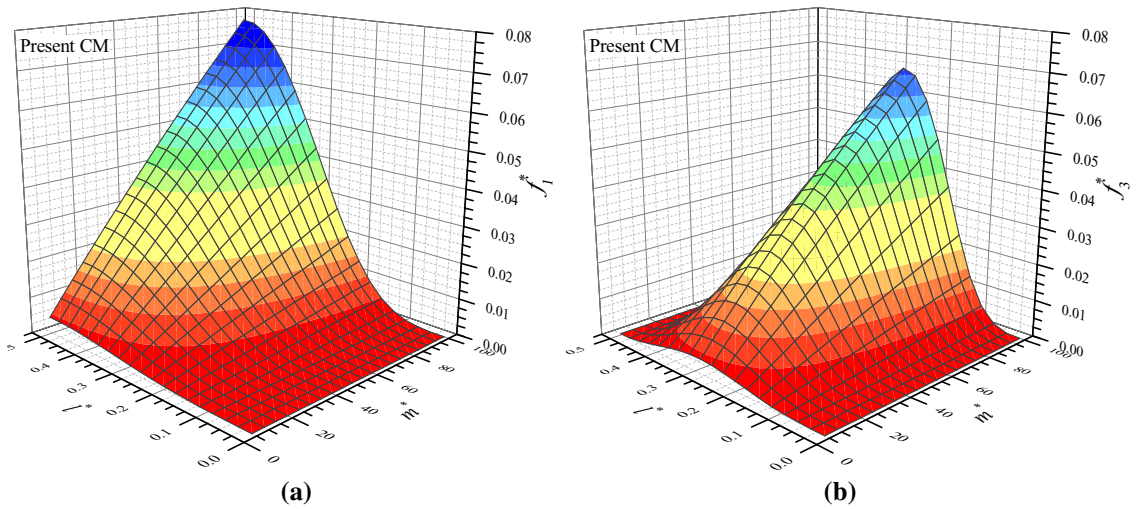

Fig. 8 Relative natural frequency shifts versus the dimensionless magnitude and position of the added mass for the **a** first and **b** second bending modes of the SWCNT-added mass vibration according to the presented CM method

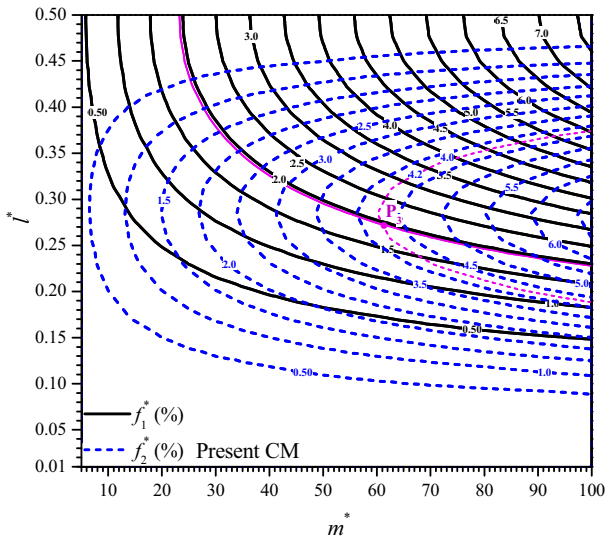

Fig. 9 Superposed contours of the relative natural frequency shifts regarding the first as well as second bending mode of the SWCNT-added mass vibration according to the presented CM method

In a similar manner, a detection contour map for SWCNT sensor may be obtained by superposing the relative natural frequency shift surfaces of Fig. 8 in common 2D diagrams. Figure 9 presents a map including the analytically estimated contours of the first and second bending modes of vibration. In order to test the identification capability of the map of Fig. 9, the natural frequency input adopted in the previous section may be used here as well. Supposing that the observed relative natural frequency shifts regarding the first and second bending modes of vibration are $f_1^* = 1.95\%$ and $f_3^* = 4.13\%$, respectively, the corresponding contours in Fig. 9 lead to the intersection point P_3 which indicates that $(m^*,\ l^*) \equiv (61,\ 0.27)$. This CM-based solution is rather dissimilar with the MM-based one $(m^*,\ l^*) \equiv (50,\ 0.2569)$, a fact that proves the necessity of taking into account the atomistic structure of the carbon nanotube in the effort to characterize its mass sensitivity.

5 Concluding remarks

Contour maps of SWCNT relative natural frequency shifts of the first and second bending modes due to an external mass attachment may provide simple identification of not only the magnitude, but also the position of the mass.

These contour maps may be established through a simple MM-based numerical method which takes into consideration the atomistic structure of the nanosensor while represents interatomic interactions with appropriate spring- and mass-like finite elements.

The information concerning the breathing as well as higher modes of the SWCNT-added mass vibration seems not to have an important contribution on simplifying the mass detection.

Despite the fact that mass detection may be realized only by adopting the bending modes of vibration, continuum mechanics theory seems to lead to rather misleading predictions.

The proposed formulation may be extended to permit identification of additional problem parameters, by introducing additional frequency data of higher modes of vibration.

Acknowledgements The authors wish to thank Mr. Arsenios Papadionisiou and Ms. Ioanna Karagianni for their help in some of the computations.

References

1. Li, X.-F., Tang, G.-J., Shen, Z.-B., Lee, K.Y.: Resonance frequency and mass identification of zeptogram-scale nanosensor based on the nonlocal beam theory. Ultrasonics **55**(1), 75–84 (2015)
2. Park, E.J., Brasuel, M., Behrend, C., Philbert, M.A., Kopelman, R.: Ratiometric optical PEBBLE nanosensors for real-time magnesium ion concentrations inside viable cells. Anal. Chem. **75**(15), 3784–3791 (2003)
3. Liao, X., Liao, Q., Zhang, Z., Yan, X., Liang, Q., Wang, Q., Li, M., Zhang, Y.A.: Highly stretchable ZnO@fiber-based multifunctional nanosensor for strain/temperature/UV detection. Adv. Funct. Mater. **26**(18), 3074–3081 (2016). 2016
4. He, R.X., Lin, P., Liu, Z.K., Zhu, H.W., Zhao, X.Z., Chan, H.L.W., Yan, F.: Solution-gated graphene field effect transistors integrated in microfluidic systems and used for flow velocity detection. Nano Lett. **12**(3), 1404–1409 (2012)
5. Chen, D., Chen, D., Zhang, T., Lawo, M., Gu, Y., Zhang, Y.: A smart scarf for pulse signal monitoring using a flexible pressure nanosensor. Proc. Int. Symp. Wearable Comput. ISWC **2666714**, 237–242 (2014)
6. Valente, J., Ou, J.-Y., Plum, E., Youngs, I.J., Zheludev, N.I.: A magneto-electro-optical effect in a plasmonic nanowire material. Nat. Commun. **6**, 7021 (2015)
7. Yang, W., Ratinac, K.R., Ringer, S.R., Thordarson, P., Gooding, J.J., Braet, F.: Carbon nanomaterials in biosensors: should you use nanotubes or graphene. Angew. Chem. Int. Ed. **49**(12), 2114–2138 (2010)
8. Artiles, M.S., Rout, C.S., Fisher, T.S.: Graphene-based hybrid materials and devices for biosensing. Adv. Drug Deliv. Rev. **63**(14–15), 1352–60 (2011)
9. Varghese, S.H., Nair, R., Nair, B.G., Hanajiri, T., Maekawa, T., Yoshida, Y., Kumar, D.S.: Sensors based on carbon nanotubes and their applications: a review. Curr. Nanosci. **6**(4), 331–346 (2010)
10. Jensen, K., Kim, K., Zettl, A.: An atomic-resolution nanomechanical mass sensor. Nat. Nanotechnol. **3**(9), 533–537 (2008)
11. Chiu, H.Y., Hung, P., Postma, H.W.C., Bockrath, M.: Atomic-scale mass sensing using carbon nanotube resonators. Nano Lett. **8**(12), 4342–4346 (2008)
12. Chaste, J., Eichler, A., Moser, J., Ceballos, G., Rurali, R., Bachtold, A.: A nanomechanical mass sensor with yoctogram resolution. Nat. Nanotechnol. **7**(5), 301–304 (2012)
13. Rafiee, R., Moghadam, R.M.: On the modeling of carbon nanotubes: a critical review. Compos. Part B Eng. **56**, 435–449 (2014)
14. Li, C., Chou, T.-W.: Single-walled carbon nanotubes as ultrahigh frequency nanomechanical resonators. Phys. Rev. B Condens. Matter Mater. Phys. **68**(7), 734051–734053 (2003)
15. Fakhrabadi, M.M.S., Amini, A., Rastgoo, A.: Vibrational properties of two and three junctioned carbon nanotubes. Comput. Mater. Sci. **65**, 411–425 (2012)
16. Fakhrabadi, M.M.S., Amini, A., Reshadi, F., Khani, N., Rastgoo, A.: Investigation of buckling and vibration properties of hetero-junctioned and coiled carbon nanotubes. Comput. Mater. Sci. **73**, 93–112 (2013)
17. Fakhrabadi, M.M.S., Khani, N., Pedrammehr, S.: Vibrational analysis of single-walled carbon nanocones using molecular mechanics approach. Phys. E Low-Dimens. Syst. Nanostruct. **44**(7–8), 1162–1168 (2012)
18. Chowdhury, R., Adhikari, S., Wang, C.Y., Scarpa, F.: A molecular mechanics approach for the vibration of single-walled carbon nanotubes. Comput. Mater. Sci. **48**(4), 730–735 (2010)
19. Ansari, R., Rouhi, H., Rajabiehfard, R.: Free vibration analysis of single-walled carbon nanotubes using semi-analytical finite element. Int. J. Comput. Methods Eng. Sci. Mech. **13**, 202–209 (2012)
20. Kim, M.H., Seo, S., Liu, W.K., Lim, B.S., Choi, J.B., Kim, M.K.: A modal analysis of carbon nanotube using elastic network model. J. Mech. Sci. Technol. **26**(11), 3433–3438 (2012)
21. Annin, B.D., Alekhin, V.V., Babichev, A.V., Korobeynikov, S.N.: Molecular mechanics method applied to problems of stability and natural vibrations of single-layer carbon nanotubes. Mech. Solids **47**(5), 544–559 (2012)
22. Lee, J.H., Lee, B.S.: Modal analysis of carbon nanotubes and nanocones using FEM. Comput. Mater. Sci. **51**(1), 30–42 (2012)
23. Kiani, K.: Nonlocal continuous models for forced vibration analysis of two- and three-dimensional ensembles of single-walled carbon nanotubes. Phys. E Low-Dimens. Syst. Nanostruct. **60**, 229–245 (2014)
24. Imani Yengejeh, S., Delgado, J.M.P.Q., De Lima, A.G.B., Öchsner, A.: Numerical simulation of the vibration behavior of curved carbon nanotubes. Adv. Mater. Sci. Eng. **2014**, 815340 (2014)
25. Imani Yengejeh, S., Akbar Zadeh, M., Öchsner, A.: Numerical modeling of eigenmodes and eigenfrequencies of hetero-junction carbon nanotubes with pentagon-heptagon pair defects. Comput. Mater. Sci. **92**, 76–83 (2014)

26. Motamedi, M., Mashhadi, M.M., Rastgoo, A.: Vibration behavior and mechanical properties of carbon nanotube junction. J. Comput. Theor. Nanosci. **10**(4), 1033–1037 (2013)
27. Gajbhiye, S.O., Singh, S.P.: Vibration characteristics of open- and capped-end single-walled carbon nanotubes using multi-scale analysis technique incorporating Tersoff-Brenner potential. Acta Mech. **226**(11), 3565–3586 (2015)
28. Askari, H., Esmailzadeh, E., Barari, A.: A unified approach for nonlinear vibration analysis of curved structures using non-uniform rational B-spline representation. J. Sound Vib. **353**, 292–307 (2015)
29. Patel, A.M., Joshi, A.Y.: Evaluating the vibrational characteristics of double walled carbon nanotubes with pinhole defects. Curr. Nanosci. **11**(3), 371–378 (2015)
30. Amjadipour, M., Dao, D.V., Motta, N.: Vibration analysis of initially curved single walled carbon nanotube with vacancy defect for ultrahigh frequency nanoresonators. Microsyst. Technol. **22**(5), 1115–1120 (2016)
31. Fakhrabadi, M.M.S., Samadzadeh, M., Rastgoo, A., Yazdi, M.H., Mashhadi, M.M.: Vibrational analysis of carbon nanotubes using molecular mechanics and artificial neural network. Phys. E Low-Dimens. Syst. Nanostruct. **44**(3), 565–578 (2011)
32. Ouakad, H.M., Younis, M.I.: Dynamic response of slacked single-walled carbon nanotube resonators. Nonlinear Dyn. **67**(2), 1419–1436 (2012)
33. Ouakad, H.M., Younis, M.I.: Natural frequencies and mode shapes of initially curved carbon nanotube resonators under electric excitation. J. Sound Vib. **330**(13), 3182–3195 (2011)
34. Joshi, A.Y., Sharma, S.C., Harsha, S.P.: Effect of chirality and atomic vacancies on dynamics of nanoresonators based on SWCNT. Sens. Rev. **31**(1), 47–57 (2011)
35. Patel, A.M., Joshi, A.Y.: Influence of atomic vacancies on the dynamic characteristics of nanoresonators based on double walled carbon nanotube. Phys. E Low-Dimens. Syst. Nanostruct. **70**, 90–100 (2015)
36. Rappe, A.K., Casewit, C.J., Colwell, K.S., Goddard, W.A., Skiff, W.M.: UFF, a full periodic table force-field for molecular mechanics and molecular dynamics simulations. J. Am. Chem. Soc. **114**, 10024–10035 (1992)
37. Cornell, W.D., Cieplak, P., Bayly, C.I., Gould, I.R., Merz Jr., K.M., Ferguson, D.M., Spellmeyer, D.C., Fox, T., Caldwell, J.W., Kollman, P.A.: A second generation force field for the simulation of proteins, nucleic acids, and organic molecules. J. Am. Chem. Soc. **117**, 5179–5197 (1995)
38. Babakov, I.M.: Theory of Vibrations. Nauka, Leningrad (1968)
39. Jafari, A., Shirvani Shah-Enayati, S., Atai, A.A.: Size dependency in vibration analysis of nano plates; one problem, different answers. Eur. J. Mech. A/Solids **59**, 124–139 (2016)